REVIEW OF RESEARCH
ISSN: 2249-894X
IMPACT FACTOR : 5.7631(UIF)
VOLUME - 11 | ISSUE - 6 | MARCH - 2022

STRUCTRAL, MAGNETIC AND FERROELECTRIC CHARACTERISTICS OF $BiFeO_3$-$MnFe_2O_4$ NANOCOMPOSITES

Bhadreshwar and Y. A. Kumar
Department of physics, CCS University Meerut.

ABSTRACT—

The $BiFeO_3$–$MnFe_2O_4$ nanocomposite was synthesized via a simple sol–gel chemical route. X-ray diffraction using CuKα radiation confirmed the formation of mixed perovskite–spinel phases with rhombohedral and cubic structures. Dielectric measurements performed at room temperature using an LCR meter (Agilent E4980A) revealed strong frequency dependence, with permittivity and dielectric loss decreasing at higher frequencies. Ferroelectric properties measured by a Marine India PE-01 loop tracer (0–6 kV/cm, 50 Hz) showed clear P–E hysteresis, confirming polarization behavior. Magnetic characterization through M–H analysis (±15 kOe) indicated enhanced saturation magnetization with increasing ferrite content. Magnetoelectric coupling evaluated using a Marine India lock-in amplifier demonstrated improved ME response. The enhanced magnetic and magnetoelectric properties highlight the composite's potential for sensor and spintronic applications.

KEYWORDS: *Nanocomposites, Multiferroic, ferroelectric phases and Manganese ferrite.*

I. INTRODUCTION

Multiferroics are a unique class of multifunctional materials that exhibit the coexistence of magnetic, electric, and ferroelastic orderings in a single system. Because of their fascinating physical properties and potential for advanced technological applications, they have attracted significant research interest in recent years [1-2]. However, single-phase multiferroic materials showing a strong magneto-electric (ME) effect are relatively rare. As a result, extensive efforts are being made to design and develop new materials with enhanced ME coupling.

Among single-phase systems, ABO_3-type perovskites have emerged as some of the most promising multiferroic materials. In these compounds, multiferroic behavior is typically achieved by introducing ferroelectric and magnetic cations at the A and B sites of the perovskite lattice. Bismuth ferrite ($BiFeO_3$, BFO), which crystallizes in a rhombohedral structure, is one of the most extensively studied single-phase multiferroics [1, 3]. It exhibits spontaneous ferroelectric polarization at room temperature along with antiferromagnetic ordering. BFO shows a high ferroelectric polarization of approximately 100 μC cm^{-2} and a Curie temperature around 1100 K. Despite these remarkable properties, the intrinsic coupling between its ferroic orders is relatively weak, which limits its practical applications [3-5].

To overcome this limitation, composite materials have been explored as an effective strategy to enhance magneto-electric coupling. Multiferroic composites often exhibit improved ME coefficients and better signal-to-noise ratios, making them suitable for device applications such as magnetic field sensors, logic devices, switches, and transducers [6-7].

Spinel ferrites are widely recognized as excellent magnetic materials for technological applications due to their favorable physical and chemical properties. They are cost-effective, exhibit low dielectric loss, and possess good magnetic performance, which makes them suitable for memory

devices and sensor applications [8-9]. Manganese ferrite ($MnFe_2O_4$, MFO) has an inverse spinel structure and is characterized by moderate saturation magnetization, good mechanical hardness, high permeability, low loss, and appreciable magnetocrystalline anisotropy. It possesses a total spin magnetic moment of about 5 μB, which is comparatively higher than many other ferrites.

However, to the best of our knowledge, there have been no reports on the synthesis and detailed investigation of $BiFeO_3$–$MnFe_2O_4$ nanocomposites prepared via the sol–gel route focusing on their multiferroic properties. Therefore, the present work aims to synthesize $BiFeO_3$–$MnFe_2O_4$ nanocomposites using the sol–gel method and to systematically study their structural, magnetic, ferroelectric, dielectric, and magneto-electric characteristics.

II. EXPERIMENTAL PROCEDURE

Synthesis of nanocomposites

The x$BiFeO_3$–(1–x)$MnFe_2O_4$ nanocomposite was synthesized using a simple chemical method via the sol–gel route. Stoichiometric amounts of $Bi(NO_3)_3{\cdot}5H_2O$, $Fe(NO_3)_3{\cdot}9H_2O$, $Mn(NO_3)_2{\cdot}4H_2O$, citric acid ($C_6H_8O_7$), and ethylene glycol were used for the preparation of the composite. In a typical procedure, the molar ratio of Bi:Mn:Fe nitrates was maintained at 1:9:19. These nitrates were dissolved in an aqueous solution of citric acid and heated at 70–80 °C under continuous stirring until a homogeneous brown clear solution was obtained.

Subsequently, an appropriate amount of ethylene glycol was added to the solution while maintaining the same temperature and constant stirring, keeping the citric acid to ethylene glycol (CA:EG) ratio at 60:40. Stirring was continued until a viscous gel was formed. The obtained gel was dried in an oven at 110 °C and then calcined in air at 600 °C for 2 hours. The resulting powder was ground using a pestle and mortar, pelletized into discs of 8 mm diameter and 1 mm thickness, and sintered at 700 °C for 2 hours to obtain dense samples suitable for electrical and magneto-electric coupling measurements.

The structural, ferroelectric, dielectric, magnetic, and magneto-electric properties of the prepared samples were investigated using various characterization techniques. Phase identification and crystallographic analysis were carried out using X-ray powder diffraction. Room-temperature magnetic measurements up to ±15 kOe were performed using a vibrating sample magnetometer (VSM). The frequency-dependent permittivity and dielectric loss were measured using an LCR meter (Agilent Technologies E4980A). Ferroelectric hysteresis (P–E) loops were recorded using a P–E loop tracer (Marine India PE-01).

III. RESULTS AND DISCUSSION

A. XRD analysis

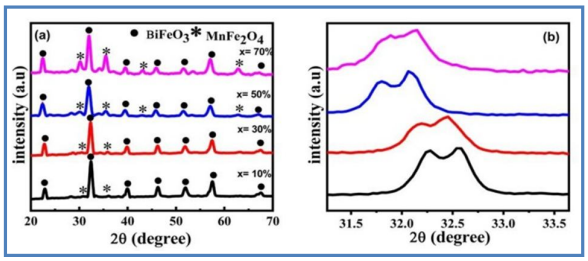

Fig. 1 (a) XRD pattern of (1-x)$BiFeO_3$-x$MnFe_2O_4$ nanocomposite with x=10%, 30%, 50% and 70% (b) Enlarged pattern of the peaks between 31.8 and 32.5.

Fig. 1(a) shows XRD pattern of the prepared (1-x) $BiFeO_3$-x$MnFe_2O_4$ nanocomposite in different composition at x = 10%, 30%, 50% and 70% respectively. The appeared diffraction peaks were indexed with the corresponding 2θ value and the recommended alignments of planes at 22.48◦(1 0 0), 32.2◦ (1 1 0), 39.49◦ (1 1 1), 45.87◦ (2 0 0), 51.49◦ (2 1 0), 57.09◦ (2 11) and 67.16◦ (2 2 0) with symbol (●)

matched well with rhombohedral structured perovskite BFO having R3C space group (#JCPDS no.72–2112). The peaks at 30.37◦ (2 2 0), 36.06◦ (3 1 1), 43.02◦ (4 0 0) and 62.94◦ (4 4 0) with symbol (*) corresponds to the spinel cubic structure of MFO (#JCPDS no 03–0864). Thus, the XRD pattern confirms the formation of composites with the presence of BFO and MFO phases. The existence of some impurity peaks of Bi36Fe2O57 (#JCPDS no.42–0181) with symbol (+) indicates the thermal instability of BFO and its chemical kinetics. It is evident from the spectra that few peaks of MFO become visible and its intensity increases with the increase in MFO content and the peaks corresponding to BFO reduces. The enlarged most intense peak of BFO phase between 31.8◦ and 32.5◦ is shifted to lower Bragg angle as displayed in Fig. 1(b). This indicates that the lattice parameters have increased due to the strain between BFO and MFO, which reveals the structural distortion in the composites [10]. This trend is compatible with the average crystallite size of nanocomposites for x = 10%, 30%, 50%, and 70%, estimated using Scherer's formula.

B. Magnetic properties

The room-temperature magnetic properties of $(1–x)BiFeO_3–xMnFe_2O_4$ nanocomposites were measured in the field range −20 kOe to +20 kOe, as shown in Fig. 2. The hysteresis loops (Fig. 2a) exhibit typical magnetic behavior, confirming ordered magnetic structure and exchange coupling between Bismuth ferrite and Manganese ferrite phases [11,12].

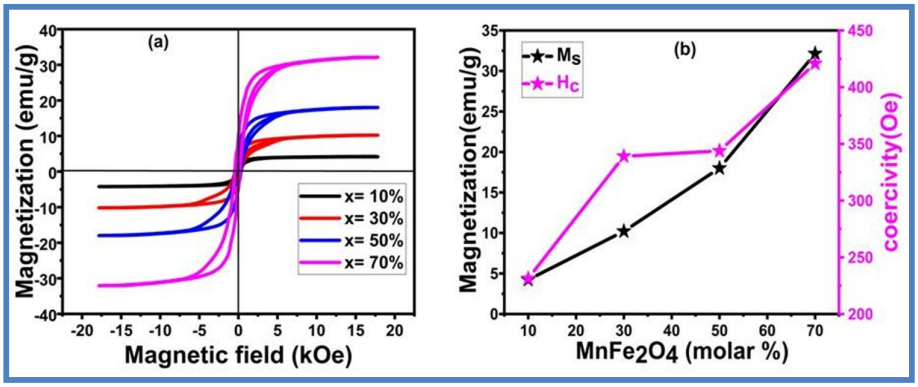

Fig. 2 (a). M - H loop of (1 - x) BiFeO3 - xMnFe2O4 nanocomposite at x = 10%, 30%, 50% & 70%. (b) Variation of coercivity (Hc) and magnetic saturation (Ms) for the (1 - x)BiFeO3 - xMnFe2O4 nanocomposites as a function of MnFe2O4 concentration

The remanence-to-saturation magnetization ratio (Mr/Ms) is less than 0.5; however, this does not rule out coupling [13]. The reduced Mr/Ms value may result from interparticle dipolar interactions, where lower particle dispersion enhances dipolar effects and decreases the ratio [13–14].

Table 1 summarizes the magnetic parameters of the prepared nanocomposites. The saturation magnetization (Ms), remanent magnetization (Mr), and coercivity (Hc) strongly depend on the content of Manganese ferrite (MFO). As the MFO concentration increases from 10% to 70%, Ms rises from 4.24 emu/g to 32.138 emu/g, while Mr increases from 0.81 emu/g to 5.55 emu/g.

Fig. 2(b) shows the variation of Hc and Ms with MFO content. The highest coercivity (420.78 Oe) and saturation magnetization (32.138 emu/g) are observed for the composite with 70% MFO. The enhancement in magnetization is attributed to improved spin alignment and interfacial exchange interactions between Bismuth ferrite and MFO phases. Additionally, stress transfer from magnetostrictive MFO to the composite interface induces polarization in BFO, further contributing to the overall increase in magnetization [11, 13].

Table 1 Magnetic parameters of (1 - x) BiFeO3 - x MnFe2O4 nanocomposites

Samples x	Ms (emu/g)	Mr (emu/g)	Hc (Oe)	Mr/ Ms	μ(μB)	K
10 %	4.2350	0.8020	231.32	0.1894	0.0231	1020.45
30 %	10.208	1.9361	339.10	0.1896	0.0527	3605.76
50 %	18.001	3.3668	420.78	0.1870	0.0876	7890.06
70%	32.138	5.5580	343.79	0.1729	0.1469	11509.08

C. Dielectric Properties

Fig. 3(a) and (b) show the variation of real (ε′) and imaginary (ε″) dielectric constants with frequency (100 Hz–2 MHz) for the composites. All samples exhibit high dielectric constant at low frequencies, which decreases with increasing frequency. This behavior is explained by Maxwell–Wagner interfacial polarization based on Koop's theory [15–16], considering the heterogeneous nature of the composite comprising Bismuth ferrite (good dielectric phase) and Manganese ferrite (low-resistive ferrite phase). At low frequencies, charge carriers accumulate at grain boundaries, leading to space charge polarization. As frequency increases, charge carriers gain sufficient energy to cross the barriers, reducing polarization and resulting in a nearly constant dielectric response at higher frequencies. Oxygen vacancies and Fe^{2+}/Fe^{3+} electron hopping also influence the dielectric behavior [17–18].

Fig. 3(c) presents the dielectric loss (tan δ) as a function of frequency. The loss decreases with increasing frequency and becomes almost frequency-independent at higher ranges. At low frequencies, dipoles follow the applied field, causing higher loss, while at higher frequencies, the lag in dipole response reduces tan δ [15, 17]. Increased MFO content enhances dielectric loss due to its lower resistivity and higher leakage conduction.

Fig. 3(d) shows the AC conductivity variation with frequency. A frequency-independent region is observed at low frequencies, followed by a sharp increase at higher frequencies due to electron hopping between grains and grain boundaries [16]. Composites with higher MFO content exhibit greater AC conductivity.

Fig. 3 Frequency dependent (a) & (b) real and imaginary dielectric constant (ε' & ε''), (c) Dielectric loss (tan δ) & (d) ac conductivity (σ_{ac}) of nanocomposites.

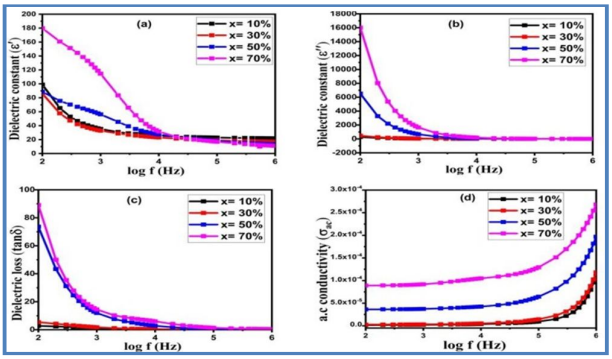

D. Impedance Analysis

Impedance spectroscopy was used to analyze the electrical behavior of the composites under AC excitation. The electrical response is described by the complex impedance, $Z^* = Z'-jZ'' = Rs-j\omega Cs$, which provides information about resistive and capacitive contributions [19]. The Nyquist plot (Z″ vs Z′) helps

in understanding charge transport, resistance, and relaxation mechanisms. Semicircular arcs in these plots indicate relaxation behavior, either Debye or non-Debye type [20].

Fig. 4(a) shows that the real part of impedance (Z′) decreases with increasing frequency up to about 10 kHz and then becomes nearly constant. This behavior is attributed to space charge polarization at grain and grain boundary interfaces. The reduction in Z′ and the corresponding increase in conductivity at higher frequencies result from the release of trapped charge carriers [19]. The maximum decrease in Z′ is observed for the composite with x = 10%.

Fig. 4(b) presents the variation of the imaginary part (Z″) with frequency. Broad and asymmetric peaks are observed, indicating relaxation processes associated with defects, immobile charge carriers, and porosity. The peak broadening confirms non-Debye type relaxation in the composites [20].

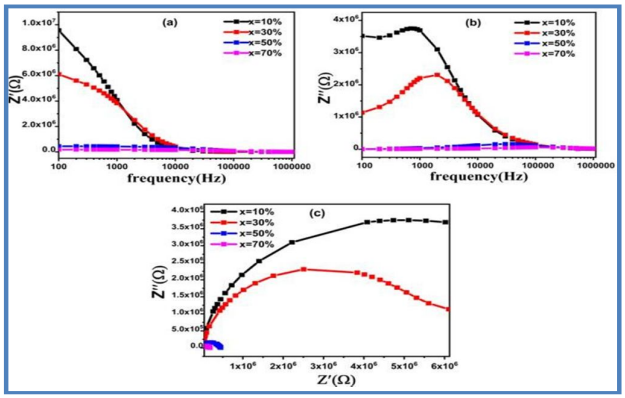

Fig. 4 Frequency dependant (a) real &(b) imaginary electrical impedance of (1 - x) BiFeO3 - xMnFe2O4 nanocomposite at x = 10%, 30%, 50% & 70% (c) Corresponding Z'' vs Z' plot.

The Nyquist plots shown in Fig. 4(c) display depressed semicircular arcs with centers below the real axis, further confirming non-Debye relaxation behavior [20]. As the content of Manganese ferrite increases, bulk resistance decreases, leading to enhanced conductivity in the Bismuth ferrite–$MnFe_2O_4$ composites [21].

E. Ferroelectric properties

To evaluate the ferroelectric properties of BFO - MFO nanocomposites, P-E loop of all the samples have been recorded within the range of electric field ±20V for frequency of 50Hz at room temperature is illustrated in Fig. 5. The unsaturated hysteresis loops evidenced very weak ferroelectric feedback in the composite system and it may be attributed to high conductive nature of the composite on account of high leakage current [22]. The countenance of ferromagnetic phase (MFO) causes this leakage current in BFO - MFO composite by the presence of oxygen vacancies and alternation of charge within Fe^{2+} and Fe^{3+}. Thus the combined effect of BFO and MFO reduces the polarization as noted is shown in Table 2. The table provides the recorded values for ferroelectric parameters include maximum polarization (Pm), remanent polarization (Pr) of (1- x)$BiFeO_3$ - x$MnFe_2O_4$ nanocomposite. The low or unsteady electric field across the sample material makes uneven dipole alignment in the direction of field; it increases leakage and hence reduces ferroelectric response [23,24].

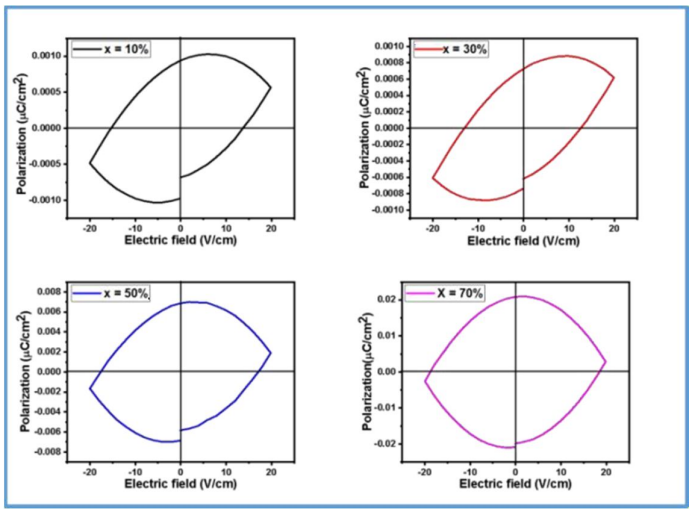

Fig. 5. P - E loop of (1- x)BiFeO3 - xMnFe2O4 nanocomposite at x = 10%, 30%, 50% & 70% recorded for frequency of 50Hz

Table 2 Ferroelectric parameters of (1 - x) $BiFeO_3$ - x $MnFe_2O_4$ nanocomposite

Samples	Pmax (μC/cm²)	Pr (μC/cm²)
X = 10 %	5.6747×10^{-4}	9.3944×10^{-4}
X = 30 %	6.1918×10^{-4}	7.3147×10^{-4}
X = 50 %	19.202×10^{-4}	6.8505×10^{-3}
X = 70%	28.8×10^{-4}	20.9536×10^{-3}

CONCLUSION

Multiferroic (1 - x)BiFeO3 - xMnFe2O4 nanocomposite in different compositions (x = 10%, 30%, 50%, 70%) were successfully synthesized by Pechini method. Rhombohedral structured perovskite BiFeO3 and Spinel cubic phase of MnFe2O4 in the composite was confirmed from X-ray diffraction pattern. The ordered magnetic structure of (1 - x)$BiFeO_3$ - x$MnFe_2O_4$ nanocomposites showed good exchange coupling interaction between two phases that is cleared with remanent ratio (M_r/M_s). Dielectric behavior of synthesized materials was realized by the interfacial phenomena of ferromagnetic and ferroelectric phases. The Nyquist's plot revealed the occurrence of non Debye relaxation in the composites. Even though, the simultaneous existence of magnetic and electric properties observed in the samples, volume fraction and resistivity of ferromagnetic material has great influence on magneto electric coupling coefficient of the studied material. These enhanced multiferroic properties of nanocomposites are highly advisable for magneto electric device applications.

REFERENCES

[1] S. Dong, J.M. Liu, S.W. Cheong, Z. Ren, Multiferroic materials and magnetoelectric physics: Symmetry, entanglement, excitation, and topology, Adv. Phys. 64 (2015) 19–626.
[2] M.M. Vopson, Fundamentals of multiferroic materials and their possible applications, Crit. Rev. Solid State Mater. Sci. 40 (2015) 223–250.
[3] Y. Li, Z. Wang, J. Yao, T. Yang, Z. Wang, J.M. Hu, C. Chen, R. Sun, Z. Tian, J. Li, L.Q. Chen, D. Viehland,

Magnetoelectric quasi-(0-3) nanocomposite heterostructures, Nat. Commun. 6 (2015) 1–7.
[4] C.W. Nan, M.I. Bichurin, S. Dong, D. Viehland, G. Srinivasan, Multiferroic magnetoelectric composites: Historical perspective, status, and future directions, J. Appl. Phys. 103 (2008).
[5] W. Prellier, M.P. Singh, P. Murugavel, The single-phase multiferroic oxides: From bulk to thin film, J. Phys. Condens. Matter. 17 (2005).
[6] N.A. Hill, Why are there so few magnetic ferroelectrics?, J. Phys. Chem. B. 104 (2000) 6694–6709.
[7] D.K. Pradhan, T.K. Nath, R.N.P. Choudhary, Dielectric, electrical and magnetic properties of PbZr 0.53Ti0.47 O3 -Ni0.65Zn 0.35Fe2O4 multiferroic composite, AIP Conf. Proc. 1372 (2011) 87–91.
[8] R.E. Newnham, D.P. Skinner, L.E. Cross, Connectivity and piezoelectric- pyroelectric composites, Mater. Res. Bull. 13 (1978) 525–536.
[9] Y. Wang, J. Hu, Y. Lin, C.W. Nan, Multiferroic magnetoelectric composite nanostructures, NPG Asia Mater. 2 (2010) 61–68.
[10] J. Shah, R.K. Kotnala, Induced magnetism and magnetoelectric coupling in ferroelectric BaTiO 3 by Cr-doping synthesized by a facile chemical route, J. Mater. Chem. A. 1 (2013) 8601–8608.
[11] J. Ou-Yang, Y. Zhang, X. Luo, B. Yan, B. Zhu, X. Yang, S. Chen, Composition dependence of the magnetic properties of CoFe2O4/CoFe2 composite nano- ceramics, Ceram. Int. 41 (2015) 3896–3900.
[12] M. Wang, X. Sun, B.Q. Geng, S.T. Zhang, Y.Q. Ma, Synthesis and magnetic properties of CoFe2/CoFe2O4 nanoparticles diluted in the MgO matrix, Mater. Res. Bull. 95 (2017) 9–16.
[13] F. Zan, Y. Ma, Q. Ma, Y. Xu, Z. Dai, G. Zheng, M. Wu, G. Li, Magnetic and impedance properties of nanocomposite CoFe2 O 4/ Co0.7 Fe0.3 and single-phase CoFe2O4 prepared via a one-step hydrothermal synthesis, J. Am. Ceram. Soc. 96 (2013) 3100–3107.
[14] F.L. Zan, Y.Q. Ma, Q. Ma, G.H. Zheng, Z.X. Dai, M.Z. Wu, G. Li, Z.Q. Sun, X.S. Chen, One-step hydrothermal synthesis and characterization of high magnetization CoFe2O4/Co0.7Fe0.3 nanocomposite permanent magnets, J. Alloys Compd. 553 (2013) 79–85.
[15] B.S. Kar, M.N. Goswami, P.C. Jana, Effects of lanthanum dopants on dielectric and multiferroic properties of BiFeO3 – BaTiO3 ceramics, J. Alloys Compd. 861 (2021) 157960.
[16] S.A. Ul Islam, F.A. Andrabi, F. Mohmed, K. Sultan, M. Ikram, K. Asokan, Ba doping induced modifications in the structural, morphological and dielectric properties of double perovskite La2NiMnO6 ceramics, J. Solid State Chem. 290 (2020).
[17] C.G. Koops, On the dispersion of resistivity and dielectric constant of some semiconductors at audiofrequencies, Phys. Rev. 83 (1951) 121–124.
[18] D. priyadarsini Jena, B. Mohanty, R.K. Parida, B.N. Parida, N.C. Nayak, Dielectric and thermal behavior of 0.75BiFeO3 - 0.25BaTiO3 filled ethylene vinyl acetate composites, Mater. Chem. Phys. 243 (2020).
[19] S. Nath, S.K. Barik, R.N.P. Choudhary, S.K. Barik, Structural, dielectric and impedance characteristics of (Sm0.5Li0.5)(Fe0.5V0.5)O3 multiferroics, Elsevier B.V., 2017.
[20] A.R. West, D.C. Sinclair, N. Hirose, Characterization of Electrical Materials, Especially Ferroelectrics, by Impedance Spectroscopy, J. Electroceramics. 1 (1997) 65–71.
[21] S. Pattanayak, A. Priyadarshan, R. Subudhi, R.K. Nayak, R. Padhee, Tailoring of electrical properties of BiFeO3 by praseodymium, J. Adv. Ceram. 2 (2013) 235– 241.
[22] A.S. Priya, I.B.S. Banu, Z. Mohammed, Effect of novel (Gd, Cu) substitution on the lectrical properties and magnetoelectric coupling of bismuth ferrite ceramics, J. Mater. Sci. Mater. Electron. 28 (2017) 8467–8472.
[23] A. Mitra, A.S. Mahapatra, A. Mallick, A. Shaw, N. Bhakta, P.K. Chakrabarti, Improved magneto-electric properties of LaFeO3 in La0.8Gd0.2Fe0.97Nb0.03O3, Ceram. Int. 44 (2018) 4442–4449.
[24] A. Sasmal, S. Sen, P.S. Devi, Synthesis and characterization of SmFeO3 and its effect on the electrical and energy storage properties of PVDF, Mater. Res. Bull. 130 (2020) 110941.